Success of prophylactic antiviral therapy for SARS-CoV-2: predicted critical efficacies and impact of different drug-specific mechanisms of action

Peter Czuppon[1,2*], Florence Débarre[1], Antonio Gonçalves[3], Olivier Tenaillon[3], Alan S. Perelson[4], Jérémie Guedj[3☯], François Blanquart[2,3☯]

1 Institute of Ecology and Environmental Sciences of Paris, Sorbonne Université, CNRS, UPEC, IRD, INRAE, 75252 Paris, France

2 Center for Interdisciplinary Research in Biology, CNRS, Collège de France, PSL Research University, 75005 Paris, France

3 Université de Paris, INSERM, IAME, F-75018 Paris

4 Theoretical Biology and Biophysics, Los Alamos National Laboratory, Los Alamos, NM 87545, USA

☯These authors contributed equally to this work.

* peter.czuppon@upmc.fr

Abstract

Repurposed drugs that are safe and immediately available constitute a first line of defense against new viral infections. Despite limited antiviral activity against SARS-CoV-2, several drugs are being tested as medication or as prophylaxis to prevent infection. Using a stochastic model of early phase infection, we evaluate the success of prophylactic treatment with different drug types to prevent viral infection. We find that there exists a critical efficacy that a treatment must reach in order to block viral establishment. Treatment by a combination of drugs reduces the critical efficacy, most effectively by the combination of a drug blocking viral entry into cells and a drug increasing viral clearance. Below the critical efficacy, the risk of infection can nonetheless be reduced. Drugs blocking viral entry into cells or enhancing viral

clearance reduce the risk of infection more than drugs that reduce viral production in infected cells. The larger the initial inoculum of infectious virus, the less likely is prevention of an infection. In our model, we find that as long as the viral inoculum is smaller than 10 infectious virus particles, viral infection can be prevented almost certainly with drugs of 90% efficacy (or more). Even when a viral infection cannot be prevented, antivirals delay the time to detectable viral loads. The largest delay of viral infection is achieved by drugs reducing viral production in infected cells. A delay of virus infection flattens the within-host viral dynamic curve, possibly reducing transmission and symptom severity. Thus, antiviral prophylaxis, even with reduced efficacy, could be efficiently used to prevent or alleviate infection in people at high risk.

Author summary

Antiviral therapy taken prophylactically can prevent a viral infection. Administering antiviral drugs in prophylaxis to health care workers or other people at risk could be especially important in the SARS-CoV-2 pandemic. Monoclonal antibodies against the SARS-CoV-2 spike protein and small molecule antiviral drugs could be used for pre- or post-exposure prophylaxis. We predict that combination therapy with two drugs with different modes of action and enough efficacy have the potential to fully prevent SARS-CoV-2 infection. We provide a prediction for the critical combination of drug efficacies above which viral establishment is suppressed entirely. Prophylactic antiviral therapy could be feasible, efficient, and alleviate the burden on healthcare systems.

Introduction

The novel coronavirus SARS-CoV-2 rapidly spread around the globe in early 2020 [1–4]. As of January 12$^{\text{th}}$ 2021, more than 91 million cases and 1.9 million associated deaths have been detected worldwide [5]. SARS-CoV-2 causes substantial morbidity and mortality with about 4% of cases being hospitalized overall, but up to 47% in the oldest age group [6–8], and a case fatality ratio of the order of 1% overall, which is again much higher in the elderly [6, 9, 10]. With a short epidemic doubling time of 2 to 7 days when uncontrolled [1, 7, 11], this epidemic can rapidly overburden healthcare systems [12].

Many countries have imposed social distancing measures to reduce incidence. Lifting these measures while keeping the epidemic in check may require a combination of intensive testing, social isolation of positive cases, efficient contact tracing and isolation of contacts [13, 14]. Even if these measures are locally successful in keeping the disease at low prevalence, the presence of SARS-CoV-2 in many countries and substantial pre-symptomatic transmission [14, 15] suggest that the virus may continue to circulate for years to come.

Existing antiviral therapies can be repurposed to treat COVID-19 in infected individuals [16–18]. Clinical trials to test several agents are underway, but existing antivirals have limited efficacy against SARS-CoV-2 and are most efficient in reducing viral load when taken early in infection [19–21]. Prophylactic therapy using (repurposed) antivirals has been proposed [22–24], is currently being tested [25] (e.g. study NCT04497987), and is successfully used in the prevention of HIV infection and malaria [26, 27]. Monoclonal antibodies, such as REGN-COV2 and Eli Lilly's bamlanivimab, both authorized for emergency use in the United States as of January 7^{th} 2021 [28], could also be used for prophylaxis. These agents could be an essential tool to reduce the probability of SARS-CoV-2 infection in individuals at high risk, e.g. the elderly (especially those in nursing homes), individuals with co-morbidities, and health care workers, thus substantially reducing the burden on health care systems. Depending on the safety profile of the antiviral drug, it could be taken pre-exposure or just after contact with an infected individual (post-exposure). In this study, we integrate recent knowledge on SARS-CoV-2 host-pathogen interactions and the mechanisms of action of the antivirals currently tested in clinical trials to evaluate the efficacy of prophylactic antiviral therapy. We calculate the probability of establishment of an infection for a given viral inoculum in an individual under prophylactic antiviral therapy.

Results

Within-host model of viral dynamics

We consider a stochastic analog of a standard target-cell-limited model for viral kinetics. In this model, infectious virus particles, V_I, infect target cells, T, i.e. cells susceptible to

infection, in the upper respiratory tract at rate β. Initially, the resulting infected cells, I_1, do not produce virus and are said to be in the eclipse phase of infection. After an average duration $1/k$, these cells exit the eclipse phase and become productively infected cells, I_2, which continuously produce virus at rate p per cell. A fraction η of these virions is infectious (V_I) and can potentially infect new target cells (T); the remainder of the produced virions, $(1-\eta)$, is non-infectious, denoted V_{NI}. Non-infectious virions may be the result of deleterious mutations, or misassembly of the virus particle. Free virions (of both types) and infected cells are lost with rate c and δ, respectively. A potential early humoral immune response could contribute to the clearance parameter c or reduce the infection rate β. In other models, the innate immune response was assumed to increase the infected cell death rate δ [21] or to reduce the number of available target cells by putting them into a refractory state [19, 29]. It is currently not possible to decide on the best model structure to describe innate immunity given the limited available data during early infection. For large numbers of target cells, infected cells and virions, the following set of differential equations describes the dynamics:

$$\begin{aligned}
\frac{dT}{dt} &= -\beta T V_I, \\
\frac{dI_1}{dt} &= \beta T V_I - k I_1, \\
\frac{dI_2}{dt} &= k I_1 - \delta I_2, \\
\frac{dV_I}{dt} &= \eta p I_2 - c V_I - \beta T V_I, \\
\frac{dV_{NI}}{dt} &= (1-\eta) p I_2 - c V_{NI}.
\end{aligned} \tag{1}$$

To generate parameter estimates for system (1), we followed the methodology of a previous study (Section S7 in the Supplementary Information (SI)) [19]. We show examples of our predictions in four out of 13 analyzed patients (Fig. 1a). An important quantity in determining the dynamics of this model is the within-host basic reproductive number R_0. It reflects the mean number of secondary cell infections caused by a single infected cell at the beginning of the infection when target cells are not limiting. Using next-generation tools for invasion analysis [30], the within-host basic

reproductive number for model (1) is given by

$$R_0 = \frac{\beta T_0}{c + \beta T_0} \frac{\eta p}{\delta}, \tag{2}$$

where T_0 is the initial number of target cells. R_0 is the product of two terms: $\beta T_0/(c + \beta T_0)$, which corresponds to the probability that the virus infects a cell before it is cleared, and $\eta p/\delta$, which is the mean number of infectious virus particles produced by an infected cell during its lifespan of average duration $1/\delta$. The mean number of overall virions produced, both infectious and non-infectious, is called the "burst size" ($N = p/\delta$). We study the within-host dynamics of SARS-CoV-2 in the early stage of an

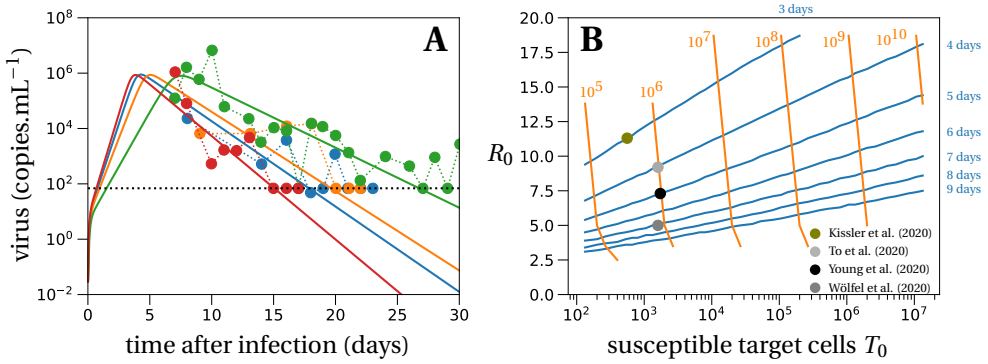

Fig 1. Deterministic within-host dynamics of SARS-CoV-2. (A) Model predictions using the target cell-limited model in four typical patients of ref. [31]. The estimated mean for the within-host R_0 of all patients from ref. [31] is 7.69. Parameter values are given in Table S2 in the Supplementary Information. The dotted line depicts the detection threshold. (B) We plot the contour lines of the viral peak time (blue lines) and the number of virus particles at the viral peak per mL (orange lines) as a function of R_0 and the number of susceptible target cells T_0. The lines are obtained by evaluating the set of differential equations in Eq. (1) with different values of T_0 (x-axis) and R_0 (y-axis). The initial amount of virus particles per mL, $V_I(0) = 1/30$, corresponds to 1 infectious virus particle in absolute numbers in the total upper respiratory tract, which we assume has a volume of 30 mL. The contour lines for viral loads (orange) stop if the viral peak is reached later than 20 days after infection, which can happen for low values of the within-host R_0. The parameters of the model are set to: $k = 5$ day^{-1}, $c = 10$ day^{-1}, $\delta = 0.595$ day^{-1}, $p = 11,200$ day^{-1}, $\eta = 0.001$ and $\beta = c\delta R_0/(T_0(\eta p - \delta R_0))$ day^{-1}. Dots depict averages of some data sets from Table 1.

infection, when the number of infected cells is small and stochastic effects are important. To do so, we define a set of reactions corresponding to the differential equations in

(1) [32, 33]:

$$
\begin{array}{lll}
V_I + T & \xrightarrow{\beta} I_1, & \text{infection of target cells,} \\
I_1 & \xrightarrow{k} I_2, & \text{end of eclipse phase,} \\
I_2 & \xrightarrow{\delta} \varnothing, & \text{infected cell death,} \\
I_2 & \xrightarrow{\eta p} I_2 + V_I, & \text{infectious virus production,} \\
I_2 & \xrightarrow{(1-\eta)p} I_2 + V_{NI}, & \text{non-infectious virus production,} \\
V_I, V_{NI} & \xrightarrow{c} \varnothing, & \text{virus clearance.}
\end{array}
\tag{3}
$$

Because we are interested in early events, we subsequently assume in the analysis that the number of target cells remains equal to T_0 (see Section S1 in the SI). This is a reasonable assumption as long as the number of infectious virions is much smaller than the number of target cells ($V_I(t) \ll T(t)$).

Parameterization of the model

The exact values of the within-host basic reproductive number R_0 and the burst size N are critical to our predictions. Based on data from 13 patients [31] with an observed peak viral load of order 10^6 virions per mL, we estimate the within-host basic reproductive number to be $R_0 = 7.69$ with the 90% confidence interval being (1.43,13.95), cf. Section S7 in the SI for more details. In ref. [19] a sensitivity analysis of the same model without distinction of infectious and non-infectious virus was conducted. This sensitivity analysis revealed that the 95% confidence interval of the within-host R_0 is (1.9,17.6), in line with other estimates of R_0 for SARS-CoV-2 in the upper respiratory tract [34]. To further explore the range of R_0 values compatible with other available data sets, we systematically solved the system of equations (1) and examined the peak viral load and the time when the peak is reached, as a function of the number of susceptible target cells T_0 and R_0, with all other parameters held constant at values given in Fig. 1B. For peak viral loads between 10^5 and 10^8 copies per mL and peak timing between 3 and 9 days, encompassing the range of average outcomes observed in multiple studies (Table 1), R_0 may vary between 3 and 13 (Fig. 1B). We note that there is substantial inter-individual variability in viral loads, and some patients present an

Table 1. Literature review of SARS-CoV-2 viral load trajectories within hosts.

Country / Setting	**# ind.**	**Mean observed peak viral load** [copies.mL^{-1}]	**Mean time of observed viral peak** [days after infection]	**Reference**
Singapore / hospital / nasopharyngeal swabs	13	10^6 (max. 3×10^8)	5-10 (a few days after symptoms)	[31]
Germany / hospital / nasopharyngeal swabs	9	7×10^5 (max. 2×10^9)	≤ 7 (already declining at admission)	[37]
mainland China / throat swabs	67	10^5 (max. 3×10^7)	≤ 5 (no increase after symptom onset)	[38]
mainland China / throat swabs	94	10^5 (max. 7×10^8)	5	[39]
Hong Kong / hospital / throat swabs	23	10^6 (max. 3×10^7)	4	[40]
France / hospital / nasopharyngeal swabs	25	6×10^8 (max. 2×10^{11})	9 (inferred in prospective study)	[41]
USA / NBA players and staff / nasopharyngeal and throat swabs	68	4×10^5 (max. 10^7)	3	[36]*

Alongside the mean observed peak viral loads, we also state the maximal peak viral loads from the cited studies (minimal values are not always provided in the references). These maximal values inform about the plausible upper bound for the within-host reproductive number R_0. *Cycle threshold (Ct) values are reported. Conversion to viral loads is according to personal communication with David Ho (Columbia University).

observed peak viral load at 10^9 copies/mL or higher [35, 36], compatible with a R_0 of 15 or more. The mean observed peak viral load across the studies surveyed was 10^6 copies/mL (Table 1).

The burst size for SARS-CoV-2 is unknown. Estimates of the burst size for other coronaviruses range from $10 - 100$ [42] to $600 - 700$ [43, 44] infectious virions. We assume that the proportion of infectious virions produced by an infected cell is $\eta = 10^{-3}$. This value is motivated by the fraction of infectious virus in an inoculum injected into rhesus macaques, $\eta = 1.33 \times 10^{-3}$ [45]. The total viral burst size is then between $10,000$ and $100,000$ virions. Such large total burst size is suggested by electron

Table 2. Model parameters used in the stochastic simulations.

Parameter set	ηp [day^{-1}]	T_0 [cells]	ηN [virions]	R_0 [cells]
LowN	11.2	4×10^4	18.8	7.69
HighN	112	4×10^3	188	7.69

Parameters not shown in the table are not changed between the simulations and are set to: $k = 5$ day^{-1}, $\delta = 0.595$ day^{-1}, $c = 10$ day^{-1}, $\eta = 10^{-3}$, $\beta = c\delta R_0/(T_0(\eta p - \delta R_0))$ day^{-1}.

microscopy showing the emergence of huge numbers of virions from cells infected by SARS-CoV-1 [46, 47] (see also [48], a webpage dedicated to SARS-CoV-2: e.g. `https://www.flickr.com/photos/niaid/49557785797/in/album-72157712914621487/`). Given the uncertainty in this parameter, we ran simulations with a small (parameter set 'LowN') and a large burst size (parameter set 'HighN'). The exact values of the LowN and HighN parameter sets are given in Table 2.

Survival and establishment of the virus within the host

As shown previously [32, 33], with the model dynamics defined in (3) the probability that a viral inoculum of size V_0 establishes an infection within the host is given by:

$$\varphi = \begin{cases} 1 - \left(1 - \frac{R_0 - 1}{\eta N}\right)^{V_I(0)}, & \text{if } R_0 \geq 1, \\ 0, & \text{if } R_0 < 1\ . \end{cases} \tag{4}$$

When $R_0 > 1$, the establishment probability increases with the size of the inoculum $V_I(0)$. Indeed, for infection to succeed, only a single infectious virus particle among $V_I(0)$ needs to establish, so the more virus particles there are initially, the more likely it is that at least one establishes. Importantly, for a given R_0, the virus establishes more easily when it has a low burst size N. Keeping the mean number of secondary cell infections R_0 constant, a virus with a smaller burst size will have a larger infectivity β or smaller clearance c, which increases the first factor of R_0 (Eq. (2)). For the same number of virions to be produced at lower burst sizes, more cells need to be involved in viral production than for large burst sizes. This mitigates two risks incurred by the virus: the risk that it does not find a cell to infect before it is cleared, and the risk that the infected cell dies early by chance. Since more cells are involved in viral production for lower burst sizes, these risks are shared over all these virus-producing cells. This

reduces the stochastic variance in viral production, which in turn results in a higher establishment probability.

Prophylactic antiviral therapy blocks establishment of the virus

Next, we investigate the effect of prophylactic antiviral drug therapy on the establishment probability of the virus during the early phase of an infection. In particular, we examine drugs with four distinct modes of action.

(i) Reducing the ability of the virus to infect cells β. This corresponds, for instance, to treatments that block viral entry, e.g. a neutralizing antibody (given as a drug) that binds to the spike glycoprotein [49].

(ii) Increasing the clearance of the virus c. This mode of action models drugs such as monoclonal antibodies that may be non-neutralizing or neutralizing and bind to circulating virus particles and facilitate their clearance by phagocytic cells [50].

(iii) Reducing viral production p. This mechanism corresponds, for example, to nucleoside analogues that prevent viral RNA replication (favipiravir, remdesivir), or to protease inhibitors (lopinavir/ ritonavir) [17].

(iv) Increasing infected cell death δ. This would describe the effect of SARS-CoV-2 specific antibodies that bind to infected cells and induce antibody-dependent cellular cytoxicity or antibody-dependent cellular phagocytosis. It would also model immunomodulatory drugs that stimulate cell-mediated immune responses, or immunotoxins such as antibody toxin conjugates that can directly kill cells [51].

We denote by ε_β, ε_c, ε_p and ε_δ the efficacies of the antiviral drugs in targeting the viral infectivity, viral clearance, viral production and infected cell death, respectively. Their values range from 0 (no efficacy) to 1 (full suppression). We neglect variations in drug concentrations over time within the host and, to be conservative, assume a constant drug efficacy corresponding to the drug efficacy at the drug's minimal concentration between doses.

Antiviral reducing viral infectivity

Antiviral drugs reducing viral infectivity β by the factor $(1-\varepsilon_\beta)$ leave the burst size N unchanged, but reduce the basic reproductive number, R_0, by a factor

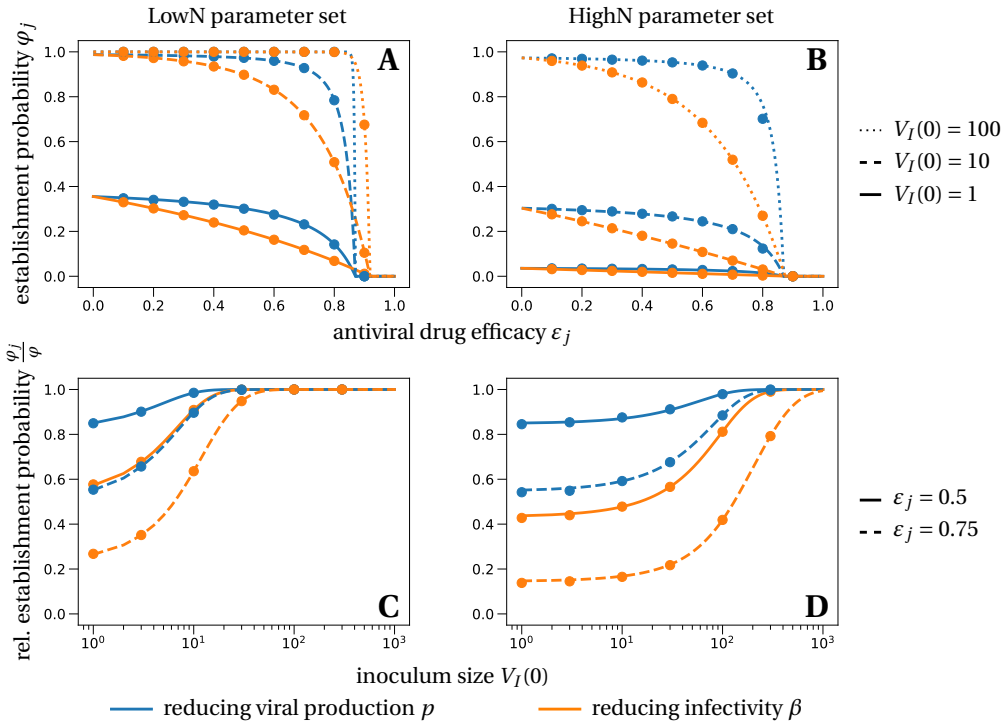

Fig 2. Establishment probability of a viral infection under prophylactic treatment with different antiviral drugs, efficacies ε and various inoculum sizes V_0. The lines in panels A and B correspond to the theoretical establishment probability under the assumption that target cell numbers are constant, for the two modes of action (reducing viral infectivity equivalent to increasing clearance, Eq. (5), in orange and reducing viral production equivalent to increasing cell death, Eq. (6), in blue). The lines in the bottom panels represent the relative probability of establishment normalized by the establishment probability in the absence of treatment from Eq. (4), i.e. φ_j/φ. Dots are averages from 100,000 individual-based simulations of the within-host model described in system (3), in which target cell numbers are allowed to vary. Parameter values are given in Table 2.

$1 - f(\varepsilon_\beta) = 1 - \frac{c\varepsilon_\beta}{c+(1-\varepsilon_\beta)\beta T_0}$. If $(1 - f(\varepsilon_\beta)) \times R_0 \geq 1$, the establishment probability changes to:

$$\varphi_\beta = 1 - \left(1 - \frac{(1 - f(\varepsilon_\beta))\, R_0 - 1}{\eta N}\right)^{V_I(0)}. \tag{5}$$

If $(1 - f(\varepsilon_\beta)) \times R_0$ is less than 1, the virus will almost surely go extinct and we have $\varphi_\beta = 0$.

With a plausible inoculum size of 10 infectious virions [52,53], we find that an efficacy (ε_β) of 81% (LowN parameter set) is necessary to reduce the establishment probability of a viral infection by 50% compared to no treatment (see Fig. 2 panels A and C). Subsequently, when we mention the efficacy of an antiviral drug reducing viral infectivity, we always refer to ε_β and not $f(\varepsilon_\beta)$.

Antiviral increasing viral clearance

Antiviral drugs that increase the clearance rate c of extracellular virus particles reduce the average lifespan of a virus by a factor $(1-\varepsilon_c)$. This changes the clearance parameter c by a factor $1/(1-\varepsilon_c)$.

With this definition of efficacy, we find that the reproductive number R_0 is reduced by the same factor as obtained for a drug reducing infectivity: $(1-f(\varepsilon_c)) = 1 - \frac{c\varepsilon_c}{c+(1-\varepsilon_c)\beta T}$. Therefore, the establishment probabilities take the same form, so that $\varphi_c = \varphi_\beta$. Consequently, we will reduce our analysis to antiviral drugs that reduce viral infectivity, keeping in mind that results for the establishment probability are equally valid for drugs increasing viral clearance.

Antiviral reducing viral production

Antiviral drugs reducing the viral production (parameter p) reduce the burst size N by a factor $(1-\varepsilon_p)$. The basic reproductive number R_0 is reduced by the same factor. If $(1-\varepsilon_p) \times R_0 \geq 1$, such drugs alter the establishment probability to:

$$\varphi_p = 1 - \left(1 - \frac{(1-\varepsilon_p)R_0 - 1}{(1-\varepsilon_p)\eta N}\right)^{V_I(0)}. \tag{6}$$

A reduction of 50% of the establishment probability compared to no treatment can be achieved with an efficacy of 85% (LowN parameter set, $V_I(0) = 10$). The efficacy needed is greater than that for antivirals targeting infectivity or viral clearance (81%) (see Fig. 2 panels A and C). Thus, for imperfect drugs that do not totally prevent establishment, drugs targeting infectivity (or clearance) are more efficient than those targeting viral production. This effect emerges from the stochastic dynamics and the reduction in viral production variance mentioned above: in the early phase, it is more important for the virus to infect many host cells than to ensure the production of a large number of virions. This insight might also affect the choice of antiviral drugs, depending on whether prophylaxis is taken pre- or post-exposure. In the case of pre-exposure, the scenario we mainly focus on and for which Eq. (4) was derived, we would recommend to prioritize drugs that increase extracellular viral clearance or reduce viral infectivity. A neutralizing monoclonal antibody such as LY-CoV555 could do both. On the other hand, if prophylactic treatment is started post-exposure, e.g. a

couple of hours after a potential between-host transmission event, the likelihood is high that cells are already infected. If cells are infected, the initial condition of our analysis is changed and drugs reducing viral production such as a SARS-CoV-2 polymerase inhibitor or protease inhibitor are more efficient in preventing the establishment of the virus than drugs targeting extracellular viral processes (clearance and target cell infection) in the LowN parameter set, cf. Section S4 in the SI.

Antiviral increasing infected cell death

Increasing the rate of death of infected cells δ by the factor $1/(1-\varepsilon_\delta)$ reduces the average lifespan of an infected cell by a factor $(1-\varepsilon_\delta)$. This has the same effect on the burst size (and consequently on R_0) as an antiviral drug reducing viral production, again due to our definition of efficacy. Therefore, the establishment probabilities are the same, $\varphi_p = \varphi_\delta$. In our analysis of establishment probabilities, we thus exclusively study antivirals affecting viral production.

Critical efficacy

Above a critical treatment efficacy, the establishment of a viral infection is not possible. This is true for all modes of action and for high and low burst sizes (Fig. 2). The critical efficacy does not depend on the initial inoculum size. It is given by the condition that the drug-modified R_0 equals 1, e.g. $(1-\varepsilon_p)R_0 = 1$ for drugs reducing viral production p. This corresponds to the deterministic threshold value for the viral population to grow. Computing the critical efficacies for both modes of action with Eq. (5) and Eq. (6), we find:

$$\widetilde{\varepsilon}_p \;=\; 1-\frac{1}{R_0} \;<\; \left(1-\frac{1}{R_0}\right)\frac{\eta N}{\eta N-1} \;=\; \widetilde{\varepsilon}_\beta\,. \tag{7}$$

They differ for the two modes of action because reducing infectivity does not proportionally reduce R_0 (Eq. (2)). Thus, drugs that reduce viral production result in a slightly lower critical efficacy, an effect that is small for a low burst size of infectious virions and not discernible with a high burst size of infectious virions (see intersections of the establishment probabilities with the x-axes in Fig. 2A and B). For example, in the HighN parameter set, we find a critical efficacy of 87% for both types of drugs.

In summary, in the range where drugs cannot totally prevent infection, drugs that target viral infectivity reduce the probability of establishment more strongly; drugs that reduce viral production can totally prevent infection at slightly lower efficacy, but this difference is extremely small when burst sizes (of infectious virions) are large.

Combination therapy

We analyze how the combination of two antiviral therapies could further impede establishment of the virus. We assume that two drugs that target different mechanisms of action lead to multiplicative effects on R_0 (Bliss independence [54]). The establishment probability and critical efficacies for the two drugs can be computed in the same way as for single drug treatments.

For example, a combination of two drugs reducing viral production p and infectivity β changes the establishment probability to

$$\varphi_{p,\beta} = 1 - \left(1 - \frac{(1 - f(\varepsilon_\beta))(1 - \varepsilon_p)R_0 - 1}{(1 - \varepsilon_p)\eta N}\right)^{V_I(0)}, \tag{8}$$

if $(1 - f(\varepsilon_\beta))(1 - \varepsilon_p)R_0 \geq 1$.

The corresponding critical pair of efficacies that prevent viral infection entirely can be computed as before by solving

$$(1 - f(\widetilde{\varepsilon}_\beta))(1 - \widetilde{\varepsilon}_p)R_0 = 1, \tag{9}$$

By the arguments from above, we can replace ε_β by ε_c and ε_p by ε_δ without changing the results. Similar calculations allow us to derive the analogous quantities if we combine drugs targeting the same mechanism of action, e.g. altering p and δ or c and β at the same time. Our analysis would also carry over to combination of drugs which target the same parameter if they interact multiplicatively. For example, two drugs reducing viral infectivity β with efficacies $\varepsilon_{\beta,1}$ and $\varepsilon_{\beta,2}$, respectively, would reduce R_0 by the factor $(1 - f(\varepsilon_{\beta,1}))(1 - f(\varepsilon_{\beta,2}))$, if they act independently.

Using two drugs of limited efficacy in combination lead to large reductions in the establishment probability compared to the single drug or no treatment scenarios. For instance, two drugs with efficacies of 65% each may completely eliminate the risk of

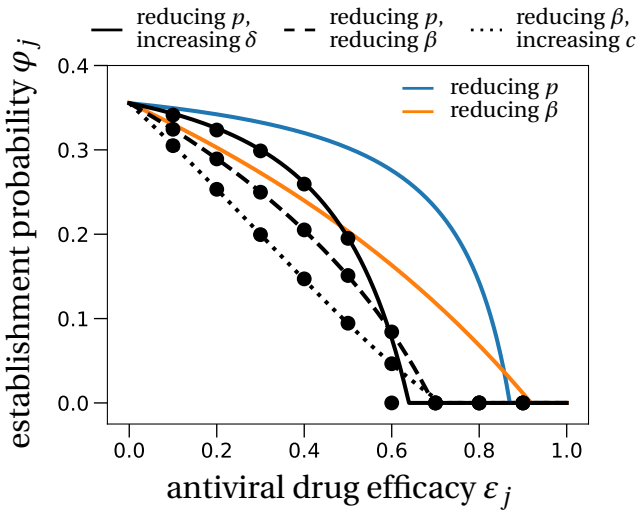

Fig 3. The effect of prophylactic combination therapy on the establishment probability. We compare different combination therapies (black lines) with the two single effect therapies (colored lines). The theoretical predictions for the combination therapies are variations of Eq. (8), adapted to the specific pair of modes of action considered. We assume that both modes of action are suppressed with the same efficacy, shown on the x-axis as ε_j. Dots are averages from 100,000 stochastic simulations using the LowN parameter set and $V_I(0) = 1$. In Section S5 in the SI, we study the effect of combination therapy in the HighN parameter set which overall leads to very similar results.

viral infection, depending on the combination used (LowN parameter set, $V_I(0) = 1$, Fig. 3). For comparison, a single drug with 65% efficacy can maximally reduce the establishment probability to $\sim 40\%$ of the no-treatment establishment probability (see Fig. 2A). We also find that, compared to the single drug cases, the critical efficacy is significantly reduced in all combinations studied.

In our analysis, we assumed that the drugs act independently (Bliss independence). This assumption may lead to an over- or underestimation of the establishment probability in case of antagonistic or synergistic drug interactions, respectively. These interactions are difficult to anticipate but were observed for HIV treatments [55].

Time to detectable viral load and extinction time

Lastly, we quantify the timescales of viral establishment and extinction of infectious virus particles. If the virus establishes, we ask whether therapy slows down its spread within the host and investigate how long it takes for the infection to reach the polymerase chain reaction (PCR) test detection threshold. Conversely, if the viral

infection does not establish, we examine how long it takes for antiviral therapy to clear all infectious virus and infected cells, which we define as the extinction time. We study all four modes of action: drugs that increase either the infected cell death rate δ or viral clearance c, and drugs reducing either viral production p or the infectivity β.

Time to detectable viral load

Even if antivirals are not efficacious enough to prevent establishment of the infection, could they still mitigate the infection? We study the effect of antiviral therapy on the time to reach a detectable viral load within the host. For example, the detection threshold in Young et al. [31] is at $10^{1.84}$ copies per mL. Assuming that the upper respiratory tract has a volume of about 30 mL [56], this corresponds to approximately $2,000$ virus particles.

In our model without treatment, the viral population size reaches $2,000$ within one day (see the leftmost data point in Fig. 4). If establishment is likely, it is best to take antiviral drugs reducing the viral production p to delay the establishment of a viral infection as long as possible. This would reduce the peak viral load [19, 21], which is presumably correlated with the severity of SARS-CoV-2 infection [57]. The time to reach a detectable viral load depends on the growth rate of the viral population, which is to the leading order $(R_0 - 1)/(\frac{1}{c+\beta T_0} + \frac{1}{k} + \frac{1}{\delta})$ (see Section S5 in the SI for a derivation). The denominator is the average duration of a virus life cycle given by the sum of the phase when virions are in the medium, the eclipse phase of infected cells, and the phase during which infected cells produce virions until their death.

Importantly, the time to reach a detectable viral load is the earliest time when a patient can be tested to determine if therapy succeeded or failed to prevent infection. That time can be increased up to 4 days for drugs inhibiting viral production p (blue line in Fig. 4), but there is significant variation with values ranging from smaller than one day to more than 10 days. Drugs reducing the infectivity β or increasing the infected cell death rate δ do not delay the establishment time. Drugs promoting viral clearance c increase the establishment time less than drugs decreasing the viral production rate p. As a brief explanation, when drugs target the infectivity or cell death, establishment occurs rapidly by full bursts of just two infected cells, which is enough to reach the detection threshold; when drugs target viral clearance or viral production,

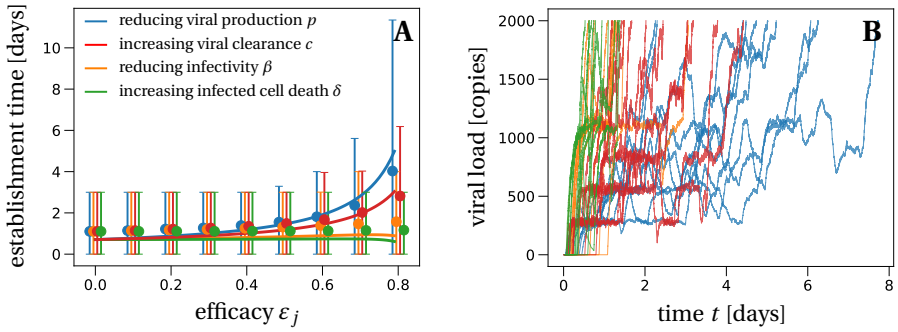

Fig 4. The mean time to reach a detectable viral load at the infection site. Panel A: Solid lines represent the theoretical prediction of the average time for the viral infection to reach 2,000 virions (see Section S6 in the SI for details). We used the LowN parameter set to simulate 10,000 stochastic simulations that reached a viral load of 2,000 total virus particles when starting with an inoculum of $V_I(0) = 1$. Dots are the average times calculated from these simulations, bars represent 90% of the simulated establishment times. We only consider efficacies below the critical efficacy ($\varepsilon_j < 0.87$, cf. Fig. 2A) because above the critical efficacy infection is never established. Panel B: We plot 10 example trajectories that reach the detectable viral load for each of the four types of treatment (efficacy $\varepsilon_j = 0.75$). Under treatment that increases the infected cell death δ or reduces infectivity β, establishing trajectories reach the detectable viral load almost immediately. In contrast, drugs that directly affect the number of virus particles, i.e. clearance c or production p, allow for trajectories that fluctuate much more, explaining the larger average detection times and the larger variation of detection times for these scenarios.

establishment may involve many more infected cells and occur slowly (SI Section S6.2).

Extinction time of infectious virus particles

Given that the infection does not establish, extinction of the within-host population of infectious virus particles typically happens within a day (in the HighN parameter set) to up to a week (in the LowN parameter set) depending on the drug's mode of action (Table 3). We find that antiviral drugs that either reduce viral infectivity β or increase the infected cell death rate δ show comparably small extinction times (Table 3). The extinction time is useful to determine the number of days a potentially infected person should take antiviral medication post-exposure.

Table 3. Establishment probabilities (φ), times to detection ($T_{\mathbf{detect}}$) and extinction time ($T_{\mathbf{ext}}$) statistics for various sets of antiviral treatment.

ε_j	**Therapy**		**LowN parameter set**		**HighN parameter set**	
			$V_0 = 1$	$V_0 = 10$	$V_0 = 1$	$V_0 = 10$
0	no treatment	φ	36%	99%	4%	30%
		T_{detect}	1 (0.5, 1.5)	0.5 (0, 0.5)	0.5 (0, 1)	0 (0, 0.5)
		T_{ext}	0 (0, 0)	1 (0, 1.5)	0 (0, 0)	0.5 (0, 0.5)
0.75	reducing p	φ	20%	89%	2%	18%
		T_{detect}	4 (2, 9)	2 (0.5, 6.5)	0.5 (0, 1)	0.5 (0, 1)
		T_{ext}	0 (0, 2)	2.5 (1, 6)	0 (0, 0)	0.5 (0, 2)
	increasing δ	φ	20%	89%	2%	18%
		T_{detect}	1 (0.5, 2)	0.5 (0, 1)	0.5 (0, 1)	0 (0, 0.5)
		T_{ext}	0 (0, 1.5)	1.5 (1, 3)	0 (0, 0)	0.5 (0, 1.5)
	reducing β	φ	9%	63%	1%	5%
		T_{detect}	1 (0.5, 2.5)	0.5 (0.5, 2)	0.5 (0, 1)	0.5 (0, 1)
		T_{ext}	0 (0, 0.5)	0.5 (0, 2.5)	0 (0, 0)	0.5 (0, 0.5)
	increasing c	φ	9%	63%	1%	5%
		T_{detect}	2.5 (1.5, 5.5)	2 (1, 5)	0 (0, 0.5)	0 (0, 0.5)
		T_{ext}	0 (0, 0)	0 (0, 2)	0 (0, 0)	0 (0, 0)
0.9	reducing p	φ	0%	0%	0%	0%
		T_{detect}	–	–	–	–
		T_{ext}	0 (0, 5)	7 (2.5, 19)	0 (0, 0.5)	0.5 (0, 5)
	increasing δ	φ	0%	0%	0%	0%
		T_{detect}	–	–	–	–
		T_{ext}	0 (0, 2)	2.5 (1, 5)	0.5 (0, 1)	0.5 (0, 2)
	reducing β	φ	1%	11%	0%	0%
		T_{detect}	1.5 (0.5, 3.5)	1 (0.5, 3)	–	–
		T_{ext}	0 (0, 0.5)	0.5 (0, 6)	0 (0, 0)	0.5 (0, 0.5)
	increasing c	φ	1%	11%	0%	0%
		T_{detect}	12 (5.5, 29)	12 (5, 28)	–	–
		T_{ext}	0 (0, 0)	0 (0, 30)	0 (0, 0)	0 (0, 0)

The first value in each cell gives the establishment probability, the second value denotes the median time to detection (days), the numbers in brackets are the 10 and 90-percentiles of the time to detection distribution (days), and the last line gives the median time to extinction (days), conditioned on non-establishment of the infection, with the 10 and 90-percentiles in brackets. The detection threshold is set to 2,000 virus particles. All times are rounded to half-day values if below 5 days, and to days if above. Missing values, denoted by dashes, are explained by the viral population not establishing; values above 30 days are set to 30. All results are estimated from 100,000 stochastic simulations for the establishment probability and 10,000 stochastic trajectories for the extinction and establishment times.

Discussion

We have investigated the effect of prophylaxis with antiviral treatments including monoclonal antibodies on the viral dynamics of SARS-CoV-2. Using a stochastic model of within-host SARS-CoV-2 dynamics whose structure and parameters are informed by

clinical data [19, 20], we showed that in principle a combination of two drugs each with efficacy between 60% and 70% will almost certainly prevent infection (Fig. 3). For single drug treatment, we find that even intermediate efficacies can block infection, most efficiently with drugs reducing infectivity β, or otherwise delay the within-host establishment of the viral infection for drugs reducing viral production p or increasing viral clearance c (Fig. 4). More generally, our stochastic model for the early phase of virus establishment within a host could be used to study the impact of prophylactic treatment on viral infections whose dynamics can be captured by the deterministic model in Eq. (1).

This model makes several important assumptions. First, it encompasses a simplified version of the innate immune response. Effects of this type of immune reaction are embedded in the parameter values of the model. For example, an early innate response, if not effectively subverted by the virus, might put some target cells into an antiviral state where they are refractory to infection, thus effectively reducing β [29], or it could reduce the viral production rate p [58]. We neglect a potential adaptive immune response against the virus because we are interested in the early stages of the infection, before the immune system develops a specific response to the viral infection. A specific immune response may in later stages enhance the ability of the body to eliminate the virus. Models that explicitly include both types of immune responses have been shown to better fit the patient data from ref. [31] when compared to models without any immune response (based on the Akaike information criterion) [21]. Our estimates of the drug efficacies needed to prevent establishment of infection are therefore conservative and in reality may be overestimates. Even if the drugs being used do not have efficacies high enough to prevent infection on their own, they can lengthen the time needed to establish infection and hence allow time for the immune response to develop and assist in the clearance of the virus. Our model also includes the removal of virus particles due to cell infections (term $-\beta V_I T$ in Eq. (1)), a process typically neglected in deterministic models of virus dynamics, e.g. [20, 21, 59, 60]. In our mechanistic approach to model virus dynamics, this term is necessary to correctly describe the early dynamics of a viral infection while the number of infectious virus particles is still low. If we were to neglect loss of infectious virus particles due to cell infections, a single virus particle could potentially infect multiple target cells. This is problematic not only in the stochastic

simulations, but also in the computation of the establishment probability of a viral infection. Lastly, we focus on the early phase of the infection in the upper respiratory tract, and neglect other compartments that may be more favorable to viral multiplication. For example, the number of virions in the sputum is (on average) 10 to 100 fold higher than in throat swabs [38]. The upper respiratory tract may allow a small amount of virus to enter the lower respiratory tract. It has also been observed in hamsters that the type of contact (airborne vs. fomite) affects the establishment probability and disease severity [61]. In future work, it would be interesting to explore the impact of this spatial structure and type of contact on viral dynamics and establishment probability.

Our results on critical efficacy, shown in Figs. 2 and 3, do not depend on the viral inoculum size and are very similar for low and high burst sizes. However, they strongly depend on the within-host basic reproductive number which we estimated at $R_0 = 7.69$. This basic reproductive number was estimated from time series of viral load in nasopharyngeal swabs in 13 infected patients [19, 31] and is consistent with the mean peak viral load observed in multiple studies (Table 1). Still, there is substantial inter-individual heterogeneity in incubation time, observed peak viral timing and load [39]. A shorter time to the viral load peak or a higher viral load peak would result in higher estimates of R_0, see for instance Fig. 1B. Yet, our qualitative findings on the effectiveness of prophylactic therapy remain valid under these variations of R_0. Of course, the quantitative predictions, which depend on R_0, change. Considering the current uncertainty in the basic reproductive number and burst size, we developed an interactive application to compute and visualize the establishment probability and deterministic dynamics as a function of parameters. This application can be used to update our results as our knowledge of within-host dynamics and treatment efficacies progresses (it can be accessed by following the instructions on `github.com/pczuppon/virus_establishment/tree/master/shiny`).

The critical efficacy above which infection is entirely prevented is the efficacy at which the within-host basic reproductive number, adjusted for the antiviral drug under consideration, passes below 1. The value of this critical efficacy could readily be obtained in a deterministic model. This theoretical value can probably be translated directly to in-vitro experiments. Yet, a translation from measured in-vitro efficacies to

in-vivo application is more challenging as studies in the context of HIV have shown: drug efficacies obtained from in-vitro experiments typically overestimate the actual in-vivo efficacy [62, 63]. Still, our stochastic framework gives several new additional insights into the probability of establishment. Importantly, below the critical efficacy, viral establishment is not certain. The establishment probability increases with the size of the initial inoculum (Fig. 2). The number of infectious virions of seasonal coronavirus in droplets and aerosol particles exhaled during 30 minutes could be in the range of 1 to 10 [52]. For SARS-CoV-2, inoculum sizes ranging from less than 10 [53] to the order of 1,000 infectious virus particles [64] have been estimated. Assuming the inoculum of infectious virus particles to be of the order of 10, in most cases the establishment of a viral infection is not ensured even with low-efficacy drugs. For efficacies below the critical efficacy, drugs reducing infectivity or increasing viral clearance reduce the establishment probability the most. Examples for this type of drug include monoclonal neutralizing antibodies that recently have shown promising results for treatment and prophylaxis of SARS-CoV-2 [65]. In contrast, drugs reducing viral production need to be close to critical efficacy to cause a marked reduction on the probability of establishment (Figs. 2 and 3). Several studies are underway to assess the prophylactic potential of repurposed drugs blocking viral production, such as lopinavir, favipiraivr or remdesivir, but there is no clear demonstration that these drugs can achieve clinically relevant antiviral efficacy [66–68].

Similar theoretical results have been obtained for HIV antiviral prophylactic treatments [69]. If initially there is one infectious HIV particle, drugs that target viral production within cells are less successful in inhibiting infection than drugs that reduce viral infection of target cells, cf. Fig. 2A in [69]. However, if the virus has already infected a cell, the difference between the two drug types vanishes, i.e., both modes of action equally reduce the establishment of an infection (Figs. 2B, 2C in [69]). In contrast, with our model we find that if there is initially one infected cell, establishment of a viral infection is suppressed more strongly by drugs that reduce viral production than by those reducing infection of target cells (Section S4 in the SI). This difference most likely arises due to the different burst sizes of infectious virus particles assumed in the two models. Here, we assume that the burst size is around 20 infectious virus particles, computed by $\eta \times N$. In contrast, the HIV model studied in [69] assumes a

burst size of 670. Indeed, increasing the burst size in our model, the HighN parameter set, recovers the result found in [69], i.e., the two different drug types affect the establishment probability equally.

Lastly, we observe that given that extinction occurs the time to extinction is largely independent of the drug's mode of action and typically occurs within a day (see Table 3). In contrast, we find a relatively strong dependence of the time to detection of an infection on the mode of action of the antiviral drug. The time to detection also strongly depends on the burst size which varies substantially depending on the assumed fraction of infectious virus particles produced, η. For example, a lower fraction than considered here in the main text will result in a higher burst size for a fixed value of R_0 (Section S7.2 in the SI) and consequently in a lower time to detection. If the delay between exposure and therapy, as well as the efficacy of the available drugs, are such that establishment of the viral infection is almost certain, antiviral drugs that reduce viral production (parameter p) will slow down the exponential growth and flatten the within-host epidemic curve the most (Fig. 4). Repurposed antiviral drugs reducing viral production were recently proposed as good drug candidates against SARS-CoV-2 [18]. This prolonged period at low viral loads could give the immune system the necessary time to activate a specific response to the virus and develop temporary host-immunity against SARS-CoV-2. This might be especially important in groups that are frequently exposed to the virus, e.g. health care workers. Still, since reducing the infection probability itself is the primary goal, drugs reducing the infectivity of virus (parameters β and c) should be favored over drugs reducing viral production (parameters p and δ) because of their stronger effect on the establishment probability (Fig. 2).

Conclusion

Clinical trials are underway to test the efficacy of several antiviral drugs [16, 17, 66, 70, 71], either as a curative treatment or as a prevention. The efficacy of repurposed drugs is in a 20-70% range [19], but better antiviral drugs might be available soon. With our model, the individual values of R_0 for the 13 untreated patients from ref. [31] range from 1.58 to 15.47 (Table S2) which approximately translates to critical efficacies between 37% and 94% in the case of drugs reducing viral

production, $\widetilde{\varepsilon}_p$ (Eq. (7)). An interactive tool has been made available to update the prediction of critical efficacies with refined parameter estimates that may come from large dataset obtained in the different target populations where prophylaxis may be relevant (such as health care workers or high-risk individuals). Given the current knowledge of SARS-CoV-2 viral dynamics, our model predicts that prophylactic antiviral therapy can block (or at least delay) a viral infection, could be administered to people at risk such as health care workers, and alleviate the burden on the healthcare systems caused by the SARS-CoV-2 pandemic.

Methods

Simulations

The individual based simulations are coded in C++ using the standard stochastic simulation algorithm for the reactions described in system (3).

Estimates for the establishment probabilities, depicted by dots in the subsequent figures, are averages of $100,000$ independent runs. Establishment was considered successful when the population size of infectious virions was at least 500. Estimates for the time to reach a detectable viral load are obtained from $10,000$ simulations where the sum of infectious and non-infectious virus particles exceeded $2,000$ copies.

The code and the data to generate the figures are available at: `github.com/pczuppon/virus_establishment`.

Supporting information

S1 Appendix. Theoretical derivations and additional analysis.

Acknowledgments

We are grateful to the INRA MIGALE bioinformatics facility (MIGALE, INRA, 2018. Migale bioinformatics Facility, doi: 10.15454/1.5572390655343293E12) for providing computational resources. We also thank Nicolas Vabret for helpful discussions on model parameterization. We thank Daniel B. Reeves, Shingo Iwami and an anonymous reviewer for comments that helped us improve our manuscript.

References

1. Li Q, Guan X, Wu P, Wang X, Zhou L, Tong Y, et al. Early Transmission Dynamics in Wuhan, China, of Novel Coronavirus–Infected Pneumonia. New England Journal of Medicine. 2020;382(13):1199–1207. doi:10.1056/NEJMoa2001316.

2. Zhu N, Zhang D, Wang W, Li X, Yang B, Song J, et al. A Novel Coronavirus from Patients with Pneumonia in China, 2019. New England Journal of Medicine. 2020;382(8):727–733. doi:10.1056/NEJMoa2001017.

3. Lai S, Bogoch I, Ruktanonchai N, Watts A, Lu X, Yang W, et al. Assessing spread risk of Wuhan novel coronavirus within and beyond China, January-April 2020: a travel network-based modelling study. medRxiv. 2020;doi:10.1101/2020.02.04.20020479.

4. Chinazzi M, Davis JT, Ajelli M, Gioannini C, Litvinova M, Merler S, et al. The effect of travel restrictions on the spread of the 2019 novel coronavirus (COVID-19) outbreak. Science. 2020;doi:10.1126/science.aba9757.

5. Dong E, Du H, Gardner L. An interactive web-based dashboard to track COVID-19 in real time. The Lancet Infectious Diseases. 2020;20(5):533 – 534. doi:https://doi.org/10.1016/S1473-3099(20)30120-1.

6. Verity R, Okell LC, Dorigatti I, Winskill P, Whittaker C, Imai N, et al. Estimates of the severity of coronavirus disease 2019: a model-based analysis. The Lancet Infectious Diseases. 2020;20(6):669–677. doi:10.1016/s1473-3099(20)30243-7.

7. Cereda D, Tirani M, Rovida F, Demicheli V, Ajelli M, Poletti P, et al. The early phase of the COVID-19 outbreak in Lombardy, Italy. arXiv:200309320 [q-bio]. 2020;.

8. Salje H, Tran Kiem C, Lefrancq N, Courtejoie N, Bosetti P, Paireau J, et al. Estimating the burden of SARS-CoV-2 in France. Science. 2020;doi:10.1126/science.abc3517.

9. Wu JT, Leung K, Bushman M, Kishore N, Niehus R, Salazar PMd, et al. Estimating clinical severity of COVID-19 from the transmission dynamics in Wuhan, China. Nature Medicine. 2020;doi:10.1038/s41591-020-0822-7.

10. Hauser A, Counotte MJ, Margossian CC, Konstantinoudis G, Low N, Althaus CL, et al. Estimation of SARS-CoV-2 mortality during the early stages of an epidemic: a modelling study in Hubei, China and northern Italy. medRxiv. 2020;doi:10.1101/2020.03.04.20031104.

11. Muniz-Rodriguez K, Chowell G, Cheung CH, Jia D, Lai PY, Lee Y, et al. Doubling Time of the COVID-19 Epidemic by Province, China. Emerging Infectious Diseases. 2020;26(8). doi:10.3201/eid2608.200219.

12. Ferguson NM, Laydon D, Nedjati-Gilani G, Imai N, Ainslie K, Baguelin M, et al. Impact of non-pharmaceutical interventions (NPIs) to reduce COVID-19 mortality and healthcare demand. Imperial College London - COVID-19 reports. 2020; Report 9.

13. Bi Q, Wu Y, Mei S, Ye C, Zou X, Zhang Z, et al. Epidemiology and transmission of COVID-19 in 391 cases and 1286 of their close contacts in Shenzhen, China: a retrospective cohort study. The Lancet Infectious Diseases. 2020;doi:10.1016/s1473-3099(20)30287-5.

14. Ferretti L, Wymant C, Kendall M, Zhao L, Nurtay A, Abeler-Dörner L, et al. Quantifying SARS-CoV-2 transmission suggests epidemic control with digital contact tracing. Science. 2020;368(6491). doi:10.1126/science.abb6936.

15. Tindale L, Coombe M, Stockdale JE, Garlock E, Lau WYV, Saraswat M, et al. Transmission interval estimates suggest pre-symptomatic spread of COVID-19. medRxiv. 2020;doi:10.1101/2020.03.03.20029983.

16. Harrison C. Coronavirus puts drug repurposing on the fast track. Nature Biotechnology. 2020;doi:10.1038/d41587-020-00003-1.

17. Li G, Clercq ED. Therapeutic options for the 2019 novel coronavirus (2019-nCoV). Nature Reviews Drug Discovery. 2020;19(3). doi:10.1038/d41573-020-00016-0.

18. Gordon DE, Jang GM, Bouhaddou M, Xu J, Obernier K, White KM, et al. A SARS-CoV-2 protein interaction map reveals targets for drug repurposing. Nature. 2020;583(7816):459–468. doi:10.1038/s41586-020-2286-9.

19. Gonçalves A, Bertrand J, Ke R, Comets E, de Lamballerie X, Malvy D, et al. Timing of antiviral treatment initiation is critical to reduce SARS-CoV-2 viral load. CPT: Pharmacometrics & Systems Pharmacology. 2020;9(9). doi:10.1002/psp4.12543.

20. Kim KS, Ejima K, Ito Y, Iwanami S, Ohashi H, Koizumi Y, et al. Modelling SARS-CoV-2 Dynamics: Implications for Therapy. medRxiv. 2020;doi:10.1101/2020.03.23.20040493.

21. Goyal A, Cardozo-Ojeda EF, Schiffer JT. Potency and timing of antiviral therapy as determinants of duration of SARS-CoV-2 shedding and intensity of inflammatory response. Science Advances. 2020;6(47):eabc7112. doi:10.1126/sciadv.abc7112.

22. Jiang S, Hillyer C, Du L. Neutralizing Antibodies against SARS-CoV-2 and Other Human Coronaviruses. Trends in Immunology. 2020;41(5):355 – 359. doi:https://doi.org/10.1016/j.it.2020.03.007.

23. Pagliano P, Piazza O, De Caro F, Ascione T, Filippelli A. Is Hydroxychloroquine a Possible Postexposure Prophylaxis Drug to Limit the Transmission to Healthcare Workers Exposed to Coronavirus Disease 2019? Clinical Infectious Diseases. 2020;doi:10.1093/cid/ciaa320.

24. Spinelli FR, Ceccarelli F, Di Franco M, Conti F. To consider or not antimalarials as a prophylactic intervention in the SARS-CoV-2 (COVID-19) pandemic. Annals of the Rheumatic Diseases. 2020;79(5):666–667. doi:10.1136/annrheumdis-2020-217367.

25. US National Library of Medicine. ClinicalTrials.gov is a database of privately and publicly funded clinical studies conducted around the world; 2020 (accessed November 12, 2020). Available from: `https://www.clinicaltrials.gov/ct2/home`.

26. Mermin J, Ekwaru JP, Liechty CA, Were W, Downing R, Ransom R, et al. Effect of co-trimoxazole prophylaxis, antiretroviral therapy, and insecticide-treated bednets on the frequency of malaria in HIV-1-infected adults in Uganda: a prospective cohort study. The Lancet. 2006;367(9518):1256–1261. doi:10.1016/S0140-6736(06)68541-3.

27. Baeten JM, Donnell D, Ndase P, Mugo NR, Campbell JD, Wangisi J, et al. Antiretroviral Prophylaxis for HIV Prevention in Heterosexual Men and Women. New England Journal of Medicine. 2012;367(5):399–410. doi:10.1056/NEJMoa1108524.

28. US Food and Drug Administration. List of Emergency Use Authorizations for treatments of COVID-19; 2021 (accessed January 7, 2021). Available from: `https://www.fda.gov/emergency-preparedness-and-response/mcm-legal-regulatory-and-policy-framework/emergency-use-authorization#coviddrugftn1`.

29. Pawelek KA, Huynh GT, Quinlivan M, Cullinane A, Rong L, Perelson AS. Modeling Within-Host Dynamics of Influenza Virus Infection Including Immune Responses. PLOS Computational Biology. 2012;8(6):1–13. doi:10.1371/journal.pcbi.1002588.

30. Hurford A, Cownden D, Day T. Next-generation tools for evolutionary invasion analyses. Journal of the Royal Society Interface. 2010;7(45). doi:10.1098/rsif.2009.0448.

31. Young BE, Ong SWX, Kalimuddin S, Low JG, Tan SY, Loh J, et al. Epidemiologic Features and Clinical Course of Patients Infected With SARS-CoV-2 in Singapore. JAMA. 2020;323(15):1488. doi:10.1001/jama.2020.3204.

32. Pearson JE, Krapivsky P, Perelson AS. Stochastic Theory of Early Viral Infection: Continuous versus Burst Production of Virions. PLOS Computational Biology. 2011;7(2):1–17. doi:10.1371/journal.pcbi.1001058.

33. Conway JM, Konrad BP, Coombs D. Stochastic Analysis of Pre- and Postexposure Prophylaxis against HIV Infection. SIAM Journal on Applied Mathematics. 2013;73(2):904–928. doi:10.1137/120876800.

34. Ke R, Zitzmann C, Ribeiro RM, Perelson AS. Kinetics of SARS-CoV-2 infection in the human upper and lower respiratory tracts and their relationship with infectiousness. medRxiv. 2020;doi:10.1101/2020.09.25.20201772.

35. Jones TC, Mühlemann B, Veith T, Biele G, Zuchowski M, Hoffmann J, et al. An analysis of SARS-CoV-2 viral load by patient age. medRxiv. 2020;.

36. Kissler SM, Fauver JR, Mack C, Tai C, Shiue KY, Kalinich CC, et al. Viral dynamics of SARS-CoV-2 infection and the predictive value of repeat testing. medRxiv. 2020;doi:10.1101/2020.10.21.20217042.

37. Wölfel R, Corman VM, Guggemos W, Seilmaier M, Zange S, Müller MA, et al. Virological assessment of hospitalized patients with COVID-2019. Nature. 2020;581(7809):465–469. doi:10.1038/s41586-020-2196-x.

38. Pan Y, Zhang D, Yang P, Poon LLM, Wang Q. Viral load of SARS-CoV-2 in clinical samples. The Lancet Infectious Diseases. 2020;20(4):411–412. doi:10.1016/S1473-3099(20)30113-4.

39. He X, Lau EHY, Wu P, Deng X, Wang J, Hao X, et al. Temporal dynamics in viral shedding and transmissibility of COVID-19. Nature Medicine. 2020;26(5):672–675. doi:10.1038/s41591-020-0869-5.

40. To KKW, Tsang OTY, Leung WS, Tam AR, Wu TC, Lung DC, et al. Temporal profiles of viral load in posterior oropharyngeal saliva samples and serum antibody responses during infection by SARS-CoV-2: an observational cohort study. The Lancet Infectious Diseases. 2020;20(5):565–574. doi:10.1016/s1473-3099(20)30196-1.

41. Tubiana S, Burdet C, Houhou N, Thy M, Manchon P, Blanquart F, et al. High-risk exposure without personal protective equipment and infection with SARS-CoV-2 in healthcare workers: results of the CoV-CONTACT prospective cohort. medRxiv. 2020;.

42. Robb JA, Bond CW. Coronaviridae. In: Fraenkel-Conrat H, Wagner RR, editors. Comprehensive Virology: Newly Characterized Vertebrate Viruses. Comprehensive Virology. Boston, MA: Springer US; 1979. p. 193–247.

43. Bar-On YM, Flamholz A, Phillips R, Milo R. SARS-CoV-2 (COVID-19) by the numbers. eLife. 2020;9. doi:10.7554/eLife.57309.

44. Hirano N, Fujiwara K, Matumoto M. Mouse Hepatitis Virus (MHV-2). Japanese Journal of Microbiology. 1976;20(3):219–225. doi:10.1111/j.1348-0421.1976.tb00978.x.

45. Munster VJ, Feldmann F, Williamson BN, van Doremalen N, Pérez-Pérez L, Schulz J, et al. Respiratory disease in rhesus macaques inoculated with SARS-CoV-2. Nature. 2020;doi:10.1038/s41586-020-2324-7.

46. Stertz S, Reichelt M, Spiegel M, Kuri T, Martínez-Sobrido L, García-Sastre A, et al. The intracellular sites of early replication and budding of SARS-coronavirus. Virology. 2007;361(2):304–315.

47. Knoops K, Kikkert M, Van Den Worm SH, Zevenhoven-Dobbe JC, Van Der Meer Y, Koster AJ, et al. SARS-coronavirus replication is supported by a reticulovesicular network of modified endoplasmic reticulum. PLoS Biol. 2008;6(9):e226.

48. National Institute of Allergy and Infectious Diseases (NIAID). SARS-CoV-2: Images and B-roll related to the novel coronavirus (SARS-CoV-2, also known as 2019-nCoV) that causes COVID-19.; 2020 (accessed November 5, 2020). Available from: `https://www.flickr.com/photos/niaid/albums/72157712914621487/with/49531042907/`.

49. Chen P, Nirula A, Heller B, Gottlieb RL, Boscia J, Morris J, et al. SARS-CoV-2 Neutralizing Antibody LY-CoV555 in Outpatients with Covid-19. New England Journal of Medicine. 2020;doi:10.1056/nejmoa2029849.

50. Igarashi T, Brown C, Azadegan A, Haigwood N, Dimitrov D, Martin MA, et al. Human immunodeficiency virus type 1 neutralizing antibodies accelerate

clearance of cell–free virions from blood plasma. Nature Medicine. 1999;5(2):211–216. doi:10.1038/5576.

51. Hoffmann RM, Mele S, Cheung A, Larcombe-Young D, Bucaite G, Sachouli E, et al. Rapid conjugation of antibodies to toxins to select candidates for the development of anticancer Antibody-Drug Conjugates (ADCs). Scientific Reports. 2020;10(1). doi:10.1038/s41598-020-65860-x.

52. Leung NHL, Chu DKW, Shiu EYC, Chan KH, McDevitt JJ, Hau BJP, et al. Respiratory virus shedding in exhaled breath and efficacy of face masks. Nature Medicine. 2020;26(5):676–680. doi:10.1038/s41591-020-0843-2.

53. Lythgoe KA, Hall M, Ferretti L, de Cesare M, MacIntyre-Cockett G, Trebes A, et al. Within-host genomics of SARS-CoV-2. medRxiv. 2020;doi:10.1101/2020.05.28.118992.

54. Chou TC. Theoretical basis, experimental design, and computerized simulation of synergism and antagonism in drug combination studies. Pharmacological Reviews. 2006;58(3):621–681. doi:10.1124/pr.58.3.10.

55. Jilek BL, Zarr M, Sampah ME, Rabi SA, Bullen CK, Lai J, et al. A quantitative basis for antiretroviral therapy for HIV-1 infection. Nature Medicine. 2012;18(3):446–451. doi:10.1038/nm.2649.

56. Baccam P, Beauchemin C, Macken CA, Hayden FG, Perelson AS. Kinetics of Influenza A Virus Infection in Humans. Journal of Virology. 2006;80(15):7590–7599. doi:10.1128/JVI.01623-05.

57. Zheng S, Fan J, Yu F, Feng B, Lou B, Zou Q, et al. Viral load dynamics and disease severity in patients infected with SARS-CoV-2 in Zhejiang province, China, January-March 2020: retrospective cohort study. BMJ. 2020;369. doi:10.1136/bmj.m1443.

58. Baccam P, Beauchemin C, Macken CA, Hayden FG, Perelson AS. Kinetics of Influenza A Virus Infection in Humans. Journal of Virology. 2006;80(15):7590–7599. doi:10.1128/JVI.01623-05.

59. Hernandez-Vargas EA, Velasco-Hernandez JX. In-host Mathematical Modelling of COVID-19 in Humans. Annual Reviews in Control. 2020;50:448–456. doi:10.1016/j.arcontrol.2020.09.006.

60. Wang S, Pan Y, Wang Q, Miao H, Brown AN, Rong L. Modeling the viral dynamics of SARS-CoV-2 infection. Mathematical Biosciences. 2020;328:108438. doi:10.1016/j.mbs.2020.108438.

61. Port JR, Yinda CK, Owusu IO, Holbrook M, Fischer R, Bushmaker T, et al. SARS-CoV-2 disease severity and transmission efficiency is increased for airborne but not fomite exposure in Syrian hamsters. medRxiv. 2020;doi:10.1101/2020.12.28.424565.

62. Pegu A, Borate B, Huang Y, Pauthner MG, Hessell AJ, Julg B, et al. A Meta-analysis of Passive Immunization Studies Shows that Serum-Neutralizing Antibody Titer Associates with Protection against SHIV Challenge. Cell Host & Microbe. 2019;26(3):336–346. doi:10.1016/j.chom.2019.08.014.

63. Reeves DB, Huang Y, Duke ER, Mayer BT, Cardozo-Ojeda EF, Boshier FA, et al. Mathematical modeling to reveal breakthrough mechanisms in the HIV Antibody Mediated Prevention (AMP) trials. PLOS Computational Biology. 2020;16(2). doi:10.1371/journal.pcbi.1007626.

64. Popa A, Genger JW, Nicholson MD, Penz T, Schmid D, Aberle SW, et al. Genomic epidemiology of superspreading events in Austria reveals mutational dynamics and transmission properties of SARS-CoV-2. Science Translational Medicine. 2020;12(573):eabe2555. doi:10.1126/scitranslmed.abe2555.

65. Baum A, Copin R, Ajithdoss D, Zhou A, Lanza K, Negron N, et al. REGN-COV2 antibody cocktail prevents and treats SARS-CoV-2 infection in rhesus macaques and hamsters. medRxiv. 2020;doi:10.1101/2020.08.02.233320.

66. Fragkou PC, Belhadi D, Peiffer-Smadja N, Moschopoulos CD, Lescure FX, Janocha H, et al. Review of trials currently testing treatment and prevention of COVID-19. Clinical Microbiology and Infection. 2020;26(8):988–998. doi:10.1016/j.cmi.2020.05.019.

67. WHO Solidarity trial consortium, Pan H, Peto R, Karim QA, Alejandria M, Henao-Restrepo AM, et al. Repurposed antiviral drugs for COVID-19 –interim WHO SOLIDARITY trial results. medRxiv. 2020;doi:10.1101/2020.10.15.20209817.

68. Beigel JH, Tomashek KM, Dodd LE, Mehta AK, Zingman BS, Kalil AC, et al. Remdesivir for the Treatment of Covid-19 — Final Report. New England Journal of Medicine. 2020;383(19):1813–1826. doi:10.1056/nejmoa2007764.

69. Duwal S, Dickinson L, Khoo S, von Kleist M. Mechanistic framework predicts drug-class specific utility of antiretrovirals for HIV prophylaxis. PLOS Computational Biology. 2019;15(1):e1006740. doi:10.1371/journal.pcbi.1006740.

70. Sheahan TP, Sims AC, Zhou S, Graham RL, Pruijssers AJ, Agostini ML, et al. An orally bioavailable broad-spectrum antiviral inhibits SARS-CoV-2 in human airway epithelial cell cultures and multiple coronaviruses in mice. Science Translational Medicine. 2020;12(541). doi:10.1126/scitranslmed.abb5883.

71. Maisonnasse P, Guedj J, Contreras V, Behillil S, Solas C, Marlin R, et al. Hydroxychloroquine use against SARS-CoV-2 infection in non-human primates. Nature. 2020;585(7826):584–587. doi:10.1038/s41586-020-2558-4.

Supplementary Information – Success of prophylactic antiviral therapy for SARS-CoV-2: predicted critical efficacies and impact of different drug-specific mechanisms of action

Peter Czuppon, Florence Débarre, Antonio Gonçalves, Olivier Tenaillon, Alan S. Perelson, Jérémie Guedj, François Blanquart

Contents

S1 Continuous virus production model

We recall the model from the main text. Infectious and non-infectious virus particles are denoted by V_I and V_{NI}, respectively, target cells by T, infected cells in the eclipse phase by I_1 and infected cells producing the virus by I_2. We use a previously studied within-host model of virus production (Pearson et al., 2011; Conway et al., 2013). The underlying individual based reactions are the following:

$$\begin{aligned}
V_I + T &\xrightarrow{\beta} I_1, && \text{infection of target cells,}\\
I_1 &\xrightarrow{k} I_2, && \text{end of eclipse phase,}\\
I_2 &\xrightarrow{\delta} \varnothing, && \text{infected cell death,}\\
I_2 &\xrightarrow{\eta p} I_2 + V_I, && \text{infectious virus production,}\\
I_2 &\xrightarrow{(1-\eta)p} I_2 + V_{NI}, && \text{non-infectious virus production,}\\
V_I, V_{NI} &\xrightarrow{c} \varnothing, && \text{virus clearance.}
\end{aligned} \tag{S1}$$

Since we model the early state within-host dynamics of a viral infection, we can assume that the number of infectious virus particles, V_I, is low so that the number of target cells is not strongly affected by transformation to infected cells, i.e. $T(t) \approx T(0) = T_0$. Then, the first reaction can be rewritten as

$$V_I \xrightarrow{\beta T_0} I_1\,. \tag{S2}$$

Using standard techniques to derive a set of ordinary differential equations from this set of reactions (e.g. Anderson and Kurtz, 2011), we find the system given in eq. (1) in the main text. Note, that in the main text we use capital letters to denote densities while here the capital letters refer to the actual numbers of cells and virus particles.

S1.1 Connection to a burst model

Since the individual based model is built on stochastic interactions of cells and virions, the number of virions produced by an infected cell is a random variable. Assuming that all virions are released at a single time, typically at cell death, the number of released virions, the burst size, follows a geometric distribution (Hataye et al., 2019). This can be seen by the following reasoning: the life-time of an infected cell is exponentially distributed with mean $1/\delta$ and during this time there is a continuous production of virions at rate p. This production, assuming that it is a Markovian process, is described by a Poisson process (see Anderson and Kurtz (2011) for the general theory of modeling chemical reactions). The probability of the

burst size, denoted by N, to be of size j is then given by the following calculation:

$$\begin{aligned}\mathbb{P}(N=j) &= \int_0^\infty \underbrace{\frac{(pt)^j}{j!}e^{-pt}}_{j \text{ virions produced until time } t} \underbrace{\delta e^{-\delta t}}_{\text{cell still alive at time } t} dt \\ &= \frac{p^j\delta}{j!}\int_0^\infty t^j e^{-(p+\delta)t}\,dt \\ &= \left(\frac{p}{p+\delta}\right)^j \frac{\delta}{p+\delta}.\end{aligned} \tag{S3}$$

This is the distribution of a geometrically distributed random variable with success probability $p/(p+\delta)$. Intuitively, the infected cell has undergone $j+1$ steps, where the initial j steps resulted in the production of a virus (term $(p/(p+\delta))^j$) and the $(j+1)$-th step was its death (term $\delta/(p+\delta)$). The mean of this geometric distribution is p/δ. The continuous-production model can therefore be seen as equivalent to a burst size model with a burst size N having a geometric distribution with mean p/δ.

S2 Burst model

The continuous-production model is more likely to be relevant for SARS-CoV-2 (Park et al., 2020), and was therefore chosen in the main text. Here we examine how a burst model would affect our findings. In a burst model, we assume that virus is produced in an infected cell but is only released to the environment upon cell death. The number of virus particles released is therefore a random number which we again denote by N.

In the corresponding reactions in Eq. (S1), we need to replace the virus production and cell death lines by

$$I_2 \xrightarrow{\delta} \eta N V_I + (1-\eta) N V_{NI}. \tag{S4}$$

In order to be consistent with the continuous-production model, we set the mean of the burst size to p/δ.

In the following we assume that the overall burst size N is Poisson-distributed. There are two reasons for this choice: (i) it is analytically relatively easy to handle, and (ii) it represents the other end of the spectrum of negative-binomially distributed burst sizes when compared to the continuous-production model which is equivalent to a geometrically-distributed burst size and thus providing an upper bound for the establishment probability of a viral infection under different forms of virus release from infected cells. A negative binomial distribution is defined by a success probability q and a dispersion parameter r. The mean is given by $qr/(1-q)$. It relates to the geometric distribution by setting $r = 1$ and to the Poisson distribution by letting $r \to \infty$. The probabilities of establishment for the continuous-production model and the Poisson-distributed burst size model represent the two extremes of negative-binomially distributed burst size models with dispersion parameter $r \in (1, \infty)$. This holds because the establishment probability can be computed by the probability generating function (Haccou et al., 2005) which is continuous and monotone in the dispersion parameter r. It is given by

$$g(z) = \left(\frac{1-q}{1-qz}\right)^r, \tag{S5}$$

where z is an auxiliary variable.

S2.1 Establishment probability

We compute the establishment probability of the virus in the burst size model. A key ingredient is the offspring distribution of a single virus particle. The offspring distribution is given by a zero-inflated Poisson distribution:

$$\begin{aligned}
\mathbb{P}(0 \text{ infectious virus offspring}) &= \underbrace{\frac{c}{c+\beta T}}_{\text{no cell infected}} + \underbrace{\frac{\beta T}{c+\beta T} e^{-\eta N}}_{\text{infected cell with 0 virions produced}}, \\
\mathbb{P}(j \text{ infectious virus offspring}) &= \frac{\beta T}{c+\beta T} \frac{(\eta N)^j}{j!} e^{-\eta N}, \quad \text{for } j \in \{1,2,3,\ldots\}.
\end{aligned} \tag{S6}$$

Note, that we are only considering infectious virus particles here because non-infectious virus particles do not affect the future virus dynamics.

The life cycle of a virus (conditioned on infecting a cell) is given by a three step process: cell infection, eclipse phase and virus production within an infected cell. Ignoring this time delay which is irrelevant if we just consider the establishment probability, the virus population can be modeled by a discrete time branching process. At each time, all infectious virions alive at the time step before produce a random number of (infectious) virions according to the offspring distribution given in eq. (S6).

The extinction probability of a time-discrete branching process, when starting with one infectious virus particle, is given by the non-trivial fixed point of the probability generating function of the offspring distribution, i.e. the fixed point in the interval $(0,1)$ (Haccou et al., 2005). The probability generating function is given by

$$g(z) = \mathbb{E}[z^{\eta N}] = \frac{c}{c+\beta T} + \frac{\beta T}{c+\beta T} e^{\eta N(z-1)}, \tag{S7}$$

where z is an auxiliary variable and $\mathbb{E}$ denotes the expectation of the random burst size of infectious virions ηN. The fixed point of this function is given as

$$z^* = \frac{c}{c+\beta T} - \frac{W\left(-\eta N \exp\left(-\eta N \frac{\beta T}{c+\beta T}\right)\right)}{\eta N}, \tag{S8}$$

where $W(x)$ is the Lambert-function (sometimes also called the product logarithm). It is defined for $x \geq -\exp(-1)$. For values below this threshold, we need to solve eq. (S7) numerically. In fact, when plotting the establishment probability in Fig. S1 below, we solve eq. (S7) numerically because the approximation of the Lambert-W function $W(x)$ is inaccurate for negative x, especially when close to $-\exp(-1)$.

The establishment probability, denoted φ, is then given by

$$\mathbb{P}(\text{virus survives}) = \varphi = 1 - \min(1, z^*)^{V_I(0)}, \tag{S9}$$

where $V_I(0)$ is the initial number of infectious virions. For alternative derivations of this result see also Pearson et al. (2011) and Conway et al. (2013).

S3 Comparison of the continuous-production and burst model

We compare the establishment probability from the burst model described above with that obtained in the continuous-production model. Redrawing the first row of Fig. 1 from the main text and comparing it with the corresponding graphs obtained from the burst model, we do not see any qualitative difference between the two models, cf. Fig. S1. As outlined in Section S2, the two studied models can be seen as the extreme values of a model continuum. By varying the dispersal parameter r of the negative binomial distribution, one can explore the entire continuum between the geometrically distributed burst size (which is equivalent to the continuous-production model) and the Poisson-distributed burst size model. Therefore, it seems safe to say that the exact mechanism by which we implement virus production in the model will only result in (minor) quantitative differences on the probability of virus establishment.

Parameter set	ηp [d^{-1}]	T_0 **[cells]**	ηN **[virions]**	R_0 **[cells]**
Low burst size (LowN)	11.2	4×10^4	18.8	7.69
High burst size (HighN)	112	4×10^3	188	7.69

Table S1: **Model parameters used in the main text and for the simulations in Fig. S1.** The remaining parameters are not changed between the simulations and are set to: $k = 5\ d^{-1}$, $\delta = 0.595\ d^{-1}$, $c = 10\ d^{-1}$, $\beta = c\delta R_0/(T_0(\eta p - \delta R_0))\ d^{-1}$, $\eta = 0.001$.

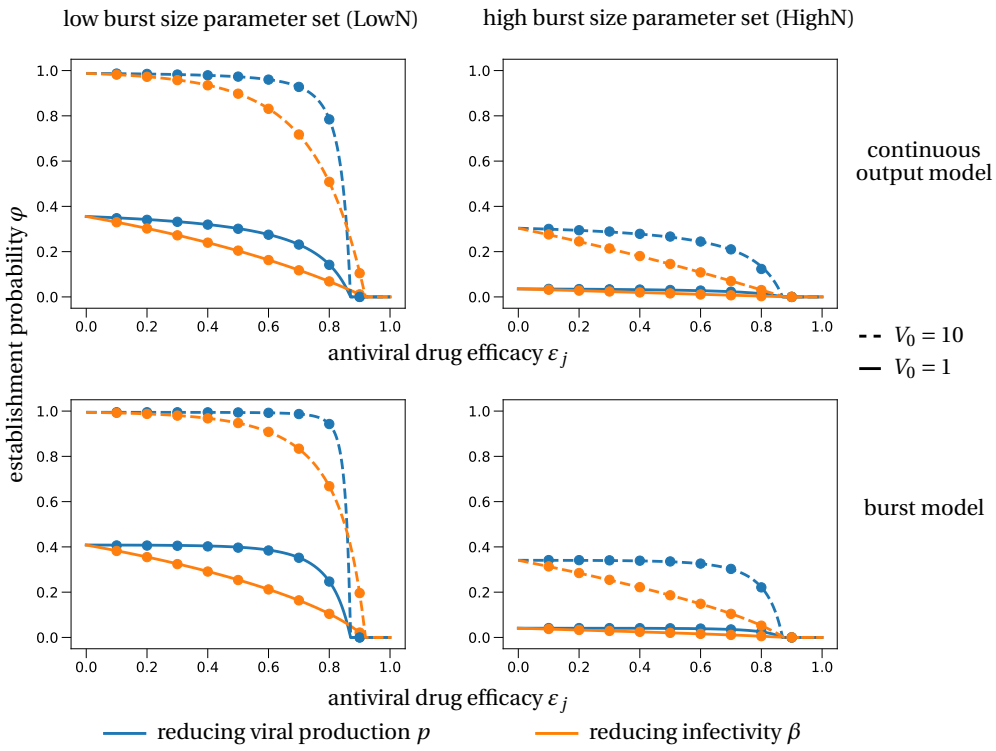

Figure S1: **Comparison of establishment probabilities in the continuous-production and burst model.** The first row is the same as the first row in Fig. 2 in the main text. The second row corresponds to the burst model. Theoretical approximations of the establishment probability for the burst model are obtained from Eq. (S9) adapted to the different scenarios.

S4 Establishment probability when starting with a single infected cell

In this section, we investigate how the establishment probability changes if treatment is started when there is already an infected cell within the host. This situation might be more realistic to post-exposure treatment where infectious virus from the initial inoculum might have already infected a target cell (if the virus was not cleared). Instead of starting with a viral inoculum, we thus need to consider the situation where an infectious cell is already producing virus (but has not yet produced an infectious virus particle). The reasoning for computing the establishment probability is then as follows: we combine the establishment probability with initially j infectious virus particles with the probability for this infected cell to produce j infectious virus particles. As we have seen in Section S1.1 the number of infectious virus particles produced by an infectious cell is geometrically distributed with success parameter $\delta/(\delta+\eta p)$. Therefore, the establishment probability when starting with an infected cell, denoted by φ_I, is given by

$$\begin{aligned}
\psi &= \sum_{j=1}^{\infty} \underbrace{\left(\frac{\eta p}{\eta p+\delta}\right)^j \left(\frac{\delta}{\eta p+\delta}\right)}_{j \text{ infectious virus particles}} \underbrace{\left(1-(1-\varphi)^j\right)}_{\text{est. prob. for } j \text{ inf. virions}} \\
&= \left(\frac{\delta}{\eta p+\delta}\right) \sum_{j=1}^{\infty} \left(\frac{\eta p}{\eta p+\delta}\right)^j \left(1-\left(1-\frac{R_0-1}{\eta N}\right)^j\right) \\
&= \frac{p(R_0-1)}{\delta N + p(R_0-1)} \\
&= 1-\frac{1}{R_0}.
\end{aligned} \tag{S10}$$

This result has also been derived in Pearson et al. (2011), where this analysis was done for the continuous-output and the burst model, and in Duwal et al. (2019) for a similar model in the context of HIV prophylaxis.

In our high burst size parameter set, there is no visible difference between treatment with a drug reducing productivity p and a drug reducing viral infectivity β (Fig. S2b). However, for the low burst size parameter set, in contrast to what we found in the main text when initializing the system with a viral inoculum, now drugs reducing the infectivity p (blue) stronger reduce the establishment probability than drugs reducing the infectivity β (orange), cf. Fig. S2a. This is explained by the order in which the drugs act: while a drug reducing viral production can immediately lower the chances for a further virus propagation, drugs reducing infectivity need to 'wait' for their targets, the extra-cellular virus, to arrive.

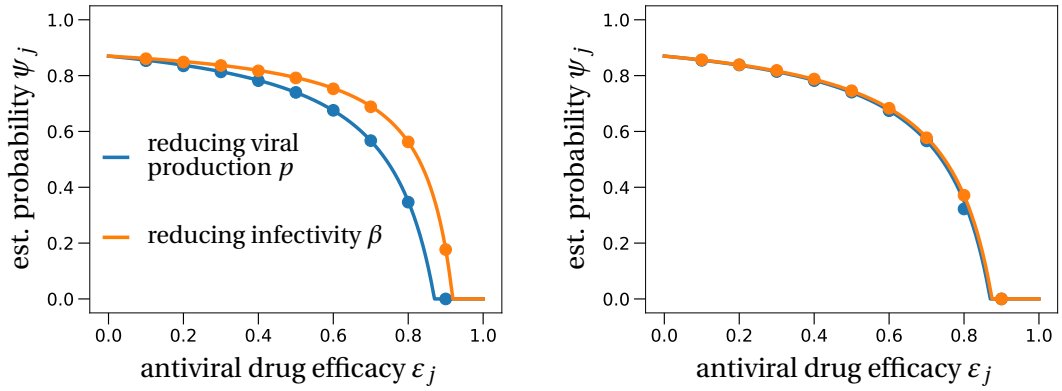

(a) LowN parameter set

(b) HighN parameter set

Figure S2: **Establishment probability when starting with a single infected cell.** We compare the theoretical prediction (solid lines) of Eq. (S10), adjusted for an antiviral drug affecting either virus productivity or virus infectivity, with stochastic simulations in the (a) LowN and (b) HighN parameter set. In the theoretical derivation of the results, target cells are fixed to their initial values. In the stochastic simulations, this number is allowed to decrease after cell infection. Averages of 10,000 realizations are depicted as dots. In contrast to the finding in the main text, in the LowN parameter set drugs reducing viral production p reduce the establishment probability stronger than antivirals reducing infectivity β. This difference becomes negligible in the HighN parameter set.

S5 Combination therapy in the HighN parameter set

We investigate the effect of combination therapy in the high burst size parameter set (Table S1). We find that the overall shape of the curves do not change compared to the LowN parameter set. A higher burst size decreases the establishment probability of the virus. If we compare Fig. S3(b) with Fig. 3 in the main text, we see that a ten-fold increase of the initial inoculum in the HighN parameter set ($V_0 = 10$) gives similar quantitative results as the LowN parameter set with $V_0 = 1$. This can be attributed to our ten-fold increase of the burst size when deriving the HighN parameter set from the LowN parameter set.

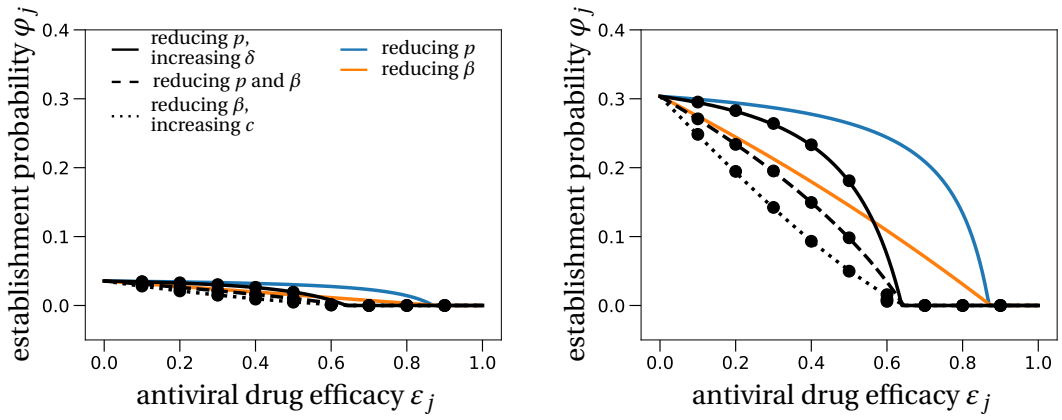

(a) $V_0 = 1$ (b) $V_0 = 10$

Figure S3: **Combination therapy in the HighN parameter set.** We plot the establishment probability of different combination therapies as was done in Fig. 3 in the main text. Dots are averages from 100,000 stochastic simulations obtained using the HighN parameter set with (a) $V_0 = 1$ or (b) $V_0 = 10$.

S6 Time to detectable viral load

In this section, we study the mean time to reach a certain amount of viral load at the infection site within the host. We approximate this time using a mixture of deterministic and stochastic arguments. Classical branching processes typically have two possible outcomes: either the process goes extinct or grows indefinitely (Haccou et al., 2005). The deterministic model is captured by the mean of such a branching process, i.e. it takes into account both possible outcomes. Therefore, if we condition the branching process on survival, the deterministic model will typically underestimate the actual size of the corresponding branching process (Desai and Fisher, 2007). One can correct this error by rescaling the deterministic process by the probability of survival. In our specific setting this means that the total number of virus particles at any time t, $V(t) = V_I(t) + V_{NI}(t)$, can be estimated as follows:

$$\begin{aligned} & \mathbb{E}[V(t)] = \varphi(t)\mathbb{E}[V(t); V(t) > 0] + (1-\varphi(t))\underbrace{\mathbb{E}[V(t); V(t) = 0]}_{=0} \\ \iff \quad & \mathbb{E}[V(t); V(t) > 0] = \frac{\mathbb{E}[V(t)]}{\varphi(t)}, \end{aligned} \tag{S11}$$

where $V(t)$ denotes the random variable for the number of virus particles at time t, $\varphi(t)$ the survival probability of the branching process until time t and $\mathbb{E}[V(t); V(t) > 0]$ the expectation of $V(t)$ for a surviving trajectory until time t.

To compute the time for the viral load to reach a certain threshold we set $\varphi(t) = \varphi$. In other words, we approximate the survival of the branching process until time t by the total establishment probability expressed in eq. (4) in the main text. This is a good approximation if the 'typical' time t to reach the threshold is large enough, so that $\varphi(t)$ is already close to the limit survival probability φ. The other term on the right-hand side in eq. (S11), the mean of the stochastic process $\mathbb{E}[V(t)]$, can be approximated by the deterministic model of the within-host model defined in eq. (1) in the main text.

As explained in the main text, we set the threshold viral load 2,000 virions (Fig. 4 in the main text). The mean time to reach this threshold value is then approximated by the time when the size $2{,}000 \times \varphi$ is reached in the deterministic model.

S6.1 Growth rate of the viral population to leading order

The exponential growth rate of the deterministic model described in eq. (1) in the main text is given by the leading eigenvalue of the system when evaluated at the origin, i.e. at zero virions Bonhoeffer et al. (1997). For efficacies close to the critical efficacy, the eigenvalue is small and can therefore be approximated by the root of a linear equation instead of a higher order polynomial. This approximation yields $\frac{R_0-1}{\frac{1}{c+\beta T_0}+\frac{1}{k}+\frac{1}{\delta}}$ as the leading eigenvalue. A *Mathematica* notebook showing this calculation is deposited at: `gitlab.com/pczuppon/virus_establishment`.

S6.2 Explaining the shape of the curves in Fig. 4 of the main text

In this section, we provide more detailed explanations about the shapes of the establishment time curves depending on the mode of action of the drug. Throughout this discussion, it is

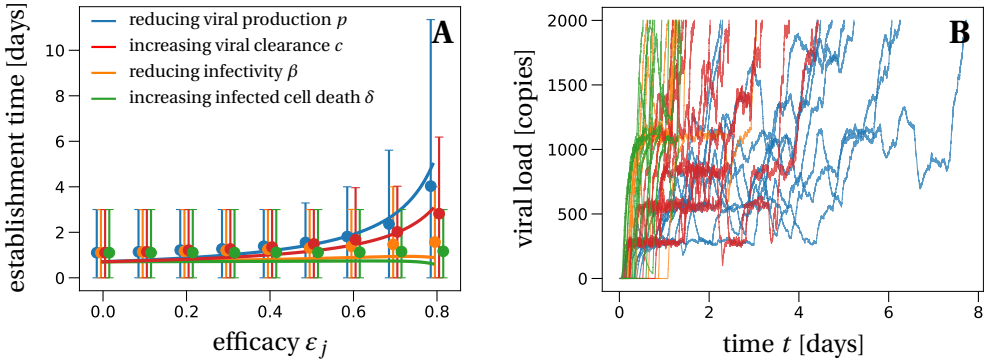

Figure S4: **The mean time to reach a detectable viral load at the infection site.** (This is Fig. 4 from the main text.) Panel A: Solid lines represent the theoretical prediction of the average time for the viral infection to reach 2,000 virions. We used the LowN parameter set to simulate 10,000 stochastic simulations that reached a viral load of 2,000 total virus particles when starting with an inoculum of $V_I(0) = 1$. Dots are the average times calculated from these simulations, error bars represent 90% of the simulated establishment times. Panel B: We plot 10 example trajectories that reach the detectable viral load for each of the four types of treatment (efficacy $\varepsilon_j = 0.75$). Under treatment that increases the infected cell death δ, establishing trajectories reach the detectable viral load almost immediately. In contrast, drugs that directly affect the number of virus, i.e. clearance c or production p, allow for trajectories that fluctuate much more, explaining the larger average detection times and the larger variation of detection times for these scenarios.

important to keep in mind that for the average establishment times, only trajectories that result in establishment are taken into account. To ease the discussion, Fig. S4 shows Fig. 4 from the main text.

Treatment that targets the virus infectivity β does not increase the establishment time because these drugs do not affect the virus dynamics itself. Conditioned on virus establishment, the initially present virus particle will infect a target cell relatively quickly, i.e., on a similar time scale than without treatment, and then follow the same dynamics as without treatment. Since the burst size largely exceeds the detection threshold, in our model just two infected cells are sufficient to reach this threshold. Therefore, the establishment time remains largely unaffected by drugs targeting the infectivity β.

For drugs increasing the infected cell death rate δ, the trajectories that contribute to the results in Fig. S4 are the ones that produced a large number of virus particles from a single cell in a short time. This is because of the strongly increased cell death rate for large values of efficacy ε_δ. Therefore, a surviving virus trajectory needs to reach large numbers of virus particles in a short time to avoid extinction. This is different for a reduced viral production p where the infected cell death rate is unaffected. Therefore, it is not necessary for a surviving

virus trajectory to reach high viral loads very quickly, even though this is of course possible which is reflected by the large 90% confidence interval. This is visualized in Fig. S4, panel B: green trajectories correspond to drugs affecting the cell death rate and blue trajectories correspond to drugs reducing viral production.

Lastly, increasing the viral clearance rate c by prophylactic treatment increases the establishment time with increasing efficacy, but not as much as treatment with drugs that reduce viral production p. The reason here is that clearance acts just after the viral production, i.e., there is time passing between the production of a virus particle and its clearance. Hence, reducing virus production has a stronger effect on the establishment time than an increase of viral clearance c which acts later in the viral life cycle.

S7 Parameter estimation

Patient data from Young et al. (2020) were fitted using the set of differential equations presented in eq. (1) in the main text. To ensure identifiability of critical parameters of the viral dynamics, i.e. the basic reproductive number R_0, the loss rate of infected cells δ and the viral production p, the remaining parameters c, k and V_0 were fixed. Viral clearance c was fixed to 10 day^{-1}. For the eclipse phase k we chose 5 day^{-1} and the initial inoculum V_0 was set to 1/30 copies.mL^{-1} (see Gonçalves et al. (2020) for further details). Parameters were estimated in a non-linear mixed effect model using the SAEM algorithm implemented in Monolix (www.lixoft.com). The best fit using all available patient data resulted in the parameter values $R_0 = 7.69$, $\delta = 0.595$ and $p = 11,200$, the principal data set used in the main text (LowN parameter set).

S7.1 Parameter estimates for individuals plotted in Fig. 1 in the main text

Applying this method to data from the 13 untreated patients in Young et al. (2020), we obtain the best parameter set for each individual. The individual parameter sets from four patients (patients 2,4,11,18) were used to plot the deterministic curves in Fig. 1A in the main text. In Fig. S5, the best fits for all 13 untreated patients are shown in separate panels with the exact parameter values given in Table S2.

Patient ID	R_0 [cells]	δ [day^{-1}]	p [day^{-1}]
2 (blue)	9.77	0.71	11,016
3	4.06	0.57	11,369
4 (orange)	8.73	0.66	11,104
6	6.72	0.58	11,281
7	1.58	0.53	11,185
8	12.11	0.48	10,817
9	15.47	0.39	10,493
11 (red)	9.2	0.86	11,060
12	8.81	0.73	11,096
14	4.45	0.78	11,396
16	7.81	0.56	11,174
17	13.43	0.73	10,679
18 (green)	7.12	0.5	11,031

Table S2: **Model parameters used for the deterministic fits in Fig. S5.** The other parameters do not vary between the individuals and are set to: $k = 5$ day^{-1}, $c = 10$ day^{-1}, $\eta = 10^{-3}$, $T_0 = 4 \times 10^4$ cells and $\beta = c\delta R_0/(T_0(\eta p - \delta R_0))$ day^{-1}. The colors (if given) correspond to the line colors of Fig. 1A in the main text.

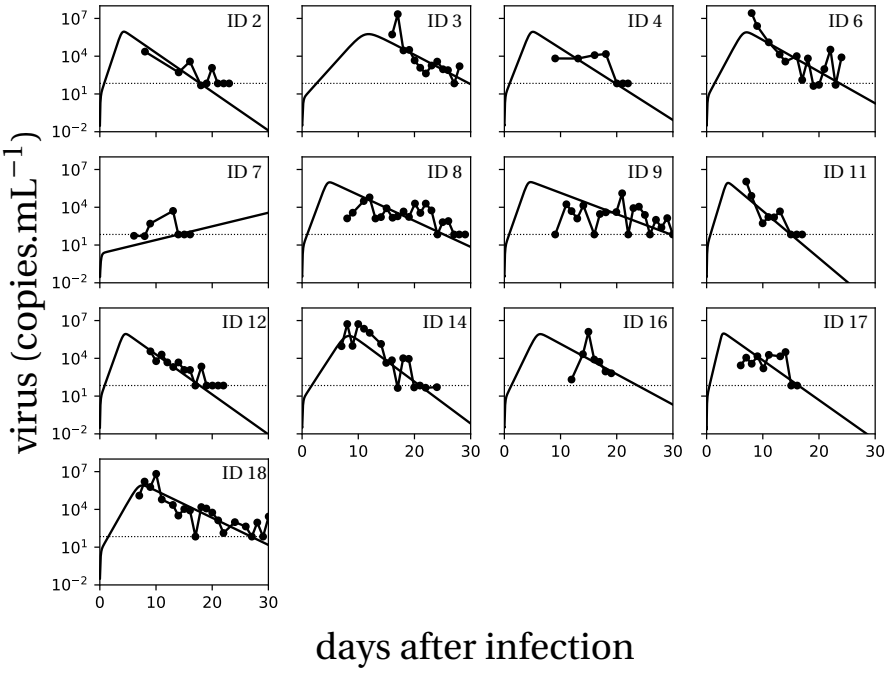

Figure S5: **Individual fits of our model to the patients from Young et al. (2020).** Model predictions using the target cell-limited model in all patients of Young et al. (2020). The estimated mean for within-host R_0 of all patients is 7.69. Individual parameter values are given in Table S2. The initial amount of virus particles per mL, $V_I(0) = 1/30$, corresponds to 1 infectious virus particle in absolute numbers in the total upper respiratory tract, which we assume has a volume of 30 mL. The dotted line depicts the detection threshold set to $10^{1.84}$.

S7.2 Sensitivity analysis with respect to variations in the fraction of infectious virus particles η

We evaluate how different choices of η, the fraction of infectious virus among all produced virus particles, affect the estimates of the within-host reproductive number R_0 and the burst size η. In the main text, we have used the parameter estimate with $\eta = 10^{-3}$ which resulted in $R_0 = 7.69$ and $N = 18,823$. For a larger fraction of infectious virus particles, $\eta = 10^{-2}$, we find $R_0 = 5.3$ and $N = 3,303$; for a smaller fraction of infectious virus particles, $\eta = 10^{-4}$, we obtain $R_0 = 9.2$ and $N = 349,367$. While the within-host reproductive number R_0 does not vary too much between the different choices of η, the burst size N shows large variation. This has no effect on our results on the establishment of a SARS-CoV-2 infection because the burst size always enters in the form of a product with η. In all the different scenarios above, the product $\eta \times N$ varies between 18 for $\eta = 10^{-3}$ and 35 for $\eta = 10^{-4}$.

Overall, the differences in estimates for R_0 will affect the precise estimate of the critical

efficacy and differences in the estimate for N translate to differences in the quantitative values of the establishment probability curves below the critical efficacy. The predictions on the detection and extinction time strongly depend on the overall burst size N so that these will vary considerably depending on the choice of η.

References

Anderson, D. F. & Kurtz, T. G. (2011), *Continuous Time Markov Chain Models for Chemical Reaction Networks*, pages 3–42. Springer New York, New York, NY. doi: 10.1007/978-1-4419-6766-4_1.

Bonhoeffer, S., May, R. M., Shaw, G. M., & Nowak, M. A. (1997). Virus dynamics and drug therapy. *Proceedings of the National Academy of Sciences*, 94(13):6971–6976. doi: 10.1073/pnas.94.13.6971.

Conway, J. M., Konrad, B. P., & Coombs, D. (2013). Stochastic analysis of pre- and postexposure prophylaxis against HIV infection. *SIAM Journal on Applied Mathematics*, 73(2):904–928. doi: 10.1137/120876800.

Desai, M. M. & Fisher, D. S. (2007). Beneficial mutation–selection balance and the effect of linkage on positive selection. *Genetics*, 176(3):1759–1798. doi: 10.1534/genetics.106.067678.

Duwal, S., Dickinson, L., Khoo, S., & von Kleist, M. (2019). Mechanistic framework predicts drug-class specific utility of antiretrovirals for HIV prophylaxis. *PLOS Computational Biology*, 15(1):e1006740. doi: 10.1371/journal.pcbi.1006740.

Gonçalves, A., Bertrand, J., Ke, R., Comets, E., de Lamballerie, X., Malvy, D., Pizzorno, A., Terrier, O., Calatrava, M. R., Mentré, F., Smith, P., Perelson, A. S., & Guedj, J. (2020). Timing of antiviral treatment initiation is critical to reduce sars-cov-2 viral load. *medRxiv*. doi: 10.1101/2020.04.04.20047886.

Haccou, P., Jagers, P., & Vatutin, V. A. (2005), *Branching Processes: Variation, Growth, and Extinction of Populations*. Cambridge Studies in Adaptive Dynamics. Cambridge University Press. doi: 10.1017/CBO9780511629136.

Hataye, J. M., Casazza, J. P., Best, K., Liang, C. J., Immonen, T. T., Ambrozak, D. R., Darko, S., Henry, A. R., Laboune, F., Maldarelli, F., Douek, D. C., Hengartner, N. W., Yamamoto, T., Keele, B. F., Perelson, A. S., & Koup, R. A. (2019). Principles governing establishment versus collapse of hiv-1 cellular spread. *Cell Host & Microbe*, 26(6):748 – 763.e20. doi: https://doi.org/10.1016/j.chom.2019.10.006.

Park, W. B., Kwon, N.-J., Choi, S.-J., Kang, C. K., Choe, P. G., Kim, J. Y., Yun, J., Lee, G.-W., Seong, M.-W., Kim, N. J., Seo, J.-S., & don Oh, M. (2020). Virus isolation from the first patient with SARS-CoV-2 in korea. *Journal of Korean Medical Science*, 35(7). doi: 10.3346/jkms.2020.35.e84.

Pearson, J. E., Krapivsky, P., & Perelson, A. S. (02 2011). Stochastic theory of early viral infection: Continuous versus burst production of virions. *PLOS Computational Biology*, 7(2):1–17. doi: 10.1371/journal.pcbi.1001058.

Young, B. E., Ong, S. W. X., Kalimuddin, S., Low, J. G., Tan, S. Y., Loh, J., Ng, O.-T., Marimuthu, K., Ang, L. W., Mak, T. M., Lau, S. K., Anderson, D. E., Chan, K. S., Tan, T. Y., Ng, T. Y., Cui, L.,

254 Said, Z., Kurupatham, L., Chen, M. I.-C., Chan, M., Vasoo, S., Wang, L.-F., Tan, B. H., Lin, R.
T. P., Lee, V. J. M., Leo, Y.-S., & Lye, D. C. (2020). Epidemiologic Features and Clinical Course
256 of Patients Infected With SARS-CoV-2 in Singapore. *JAMA*. doi: 10.1001/jama.2020.3204.